Jurnal Teknologi

Full paper

Simulation of Drying for Multilayer Membranes

Zawati Harun[a*], Tze Ching Ong[a], Ahmad Fauzi Ismail[b]

[a]*University Tun Hussien Onn, Parit Raja, 86400, Batu Pahat, Johor, Malaysia*
[b]*Advanced Membrane Technology Research Centre (AMTEC), Universiti Teknologi Malaysia, 81310 UTM Johor Bahru, Johor, Malaysia*

*Corresponding author: zawati@uthm.edu.my

Article history

Received :15 September 2013
Received in revised form :
17 November 2013
Accepted :15 January 2014

Graphical abstract

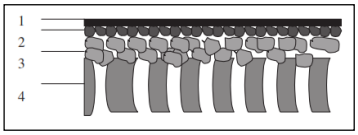

Abstract

In ceramic membrane preparation, drying variables and its phenomena are very important to ensure no defects and failures in membrane layers. Generally, ceramic membrane consists of several layer with the top structure or layers possesses a very hygroscopic zone that acting as a separator while next two layers are non hygroscopic zone. Combination of these two different multilayer systems that exhibit different properties always associated to the failure of ceramic consolidation structure during the drying and sintering process. Therefore,controlling of drying behavior is very important to ensure a consistent shrinkage exist between these two layers system. Thus in this present work, the drying process of multilayer materials was studied and observed via simulation technique. A two dimensional mathematical model that coupled mass, heat and gas transfer was employed. Finite element method was used to solve the model and numerically compute using Skyline solver to capture highly nonlinear and transient process. The results showed that drying of multilayer material for membrane structure is obviously different from drying of single layer system. Separation zone that acting as hygroscopic zone does play its roles towards effecting higher pore water pressure and gas pressure. Thus, different drying factors can be seen in the layering system. Hence, understanding those drying factors that may cause inhomogeneous shrinkage due to the existence of different porous network in membrane layers is essential to avoid ceramic membrane failure.

Keywords: Multilayer; hygroscopic; non hygroscopic; convective drying

1.0 INTRODUCTION

Theoretically, membrane can be divided into several layers as shown in Figure 1.

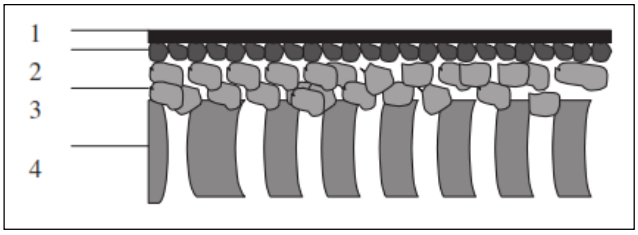

Figure 1 Schematic representation of an asymmetric membrane (extracted from Li, 2007[1])

The first top layer with fine pore structure is used as a filter for separation process.[1] The next three layers which are intermediate and bottom layer is fabricated in the form of porous structure to support the membrane itself and to ease the permeation process.[1] Obviously, top separation layer with a fine porous structure possess a hygroscopic property compared to the intermediate and bottom layer that has to be porous structure and tend to be in a non hygroscopic zone. Both layers that have different properties will generate different shrinkage mechanism especially during the drying stage.

Drying is one of the processes of ceramic membranes preparation which occurs after the precursor formation before the sintering process. As one of the most energy intensive processes in industrial,[2] drying configuration is also the less understood as it involves a lot of variables that change concurrently as the phase and stage changes.[3,4] Further complications arise if drying involves materials of multilayer.[5,6,7,8] Ceramic membranes layers as aforementioned with hygroscopic layer involve bound water mechanism that is strongly attached to capillary wall. This strongly attached water is quite difficult to measure using experimental technique due to its strong capillarity suction and high permeability value compared to the non hygroscopic material. Typically, drying of membrane layering structure not just involve the compatible issue of drying parameter but the different materials that acts with different properties also strongly influence the consistency

of shrinkage geometry which is often associated to leaking of membrane due to the failure of drying and firing processes. Drying induced nonuniform stresses such as pressure gradient of the flow of liquid during shrinkages in constant rate period (CRP), macroscopic pressure gradient of escaping gasses during falling rate period (FRP) and different thermal expansion of ceramic that may cause warping or cracking.[9] The flow of liquid, the macroscopic pressure gradient, and the temperature gradient are controlled by the drying rate and rate of drying and are typically controlled by external conditions.[9] Therefore, understanding of stages and variables that evolve with time throughout the drying is essential to eliminate all the unnecessary trouble especially for membrane application.

In this present study, a mathematical model of drying process with coupled mass, heat and gas transfer for ceramic materials has been developed. This model will emphasize on the transport mechanism of liquid by capillary action, vapor by diffusion and gas by vapor diffusion and bulk air flow in convective drying condition. The introduction of bound water on later period (FRP2) of drying was incorporated by referring previous related work.[10] Material slab used has been divided into two layers, hygroscopic and non hygroscopic layer which assemble a membranes layering systems.

2.0 MATHEMATICAL MODELING

2.1 Theoritical Formulation

In the model, the water is represented with the dissolved vapor and air are considered in liquid phase, whilst, binary mixture of vapor and dry air is considered a gas phase. Capillarity for liquid phases, diffusion by vapor and air, gas transport and also heat transport are taken into account as these phenomena represent the drying process. For hygroscopic materials, bound water is the transport mechanism in the FRP2.[10,11] Based on those analyses, governing equations are expressed into three primary variables; water pressure, P_l, temperature, T and gas pressure, P_g.

$$\frac{\partial(\phi\rho_l S_l)}{\partial t}+\frac{\partial(\phi\rho_v S_g)}{\partial t}=-\nabla.(\rho_l V_l)-\nabla.(\rho_v V_v)-\nabla.(\rho_v V_g)-\nabla.(\rho_l V_b) \quad (1)$$

For water velocity, V_l and gas velocity, V_g can be easily derived from Darcy's law[5,7]

$$V_l=-\frac{Kk_l}{\mu_l}\left[\nabla\left(P_l+Z\right)\right] \quad (2)$$

$$V_g=-\frac{Kk_g}{\mu_g}\left[\nabla\left(P_g\right)\right] \quad (3)$$

where Z is the vertical elevation from a datum. Meanwhile vapor velocity by diffusion is defined as;

$$V_v=\frac{-D_{atm}v\alpha\theta_a}{\rho_v}.\nabla\rho_v \quad (4)$$

where D_{atm} ,v , α, θ_a are the molecular diffusivity of water vapor through dry air, mass-flow factor, tortuosity factor and volumetric air term respectively. Rearranging the above equation according to the measured variables gives;

$$V_v=\frac{-D_{atm}v\alpha\theta_a}{\rho_v}\left\{\rho_o\frac{\partial h}{\partial P_l}\nabla P_l+(\rho_o+h\beta)\frac{\partial h}{\partial T}\nabla T+\rho_o\frac{\partial h}{\partial P_g}\nabla P_g\right\} \quad (5)$$

When water content reached the maximum irreducible water content, the bound water flux is taken into account into equation. The bound water velocity was derived from[10] as;

$$V_b=-D_b\nabla\theta_b \quad (6)$$

where D_b , θ_b are the bound water conductivity and volumetric bound water term respectively. Rearranging the above equation according to the measured variables gives;

$$V_b=-D_b\phi\left(\frac{\partial S_l}{\partial P_l}\nabla P_l+\frac{\partial S_l}{\partial T}\nabla T+\frac{\partial S_l}{\partial P_g}\nabla P_g\right) \quad (7)$$

By applying a mass balance to the flow of dry air within the pores of the material body dictates that the time derivative of the dry air content is equal to the spatial derivative of the dry air flux.

$$\frac{\partial(\phi\rho_a S_g)}{\partial t}=-\nabla(\rho_a V_g-\rho_v V_v) \quad (8)$$

The effect of conduction, latent heat and convection are considered in the energy equation as given as below;

$$\frac{\partial((1-\phi)c_p\rho_s+\sum_{i=a,l,v}\phi s_i\rho_i c_i)}{\partial t}=\nabla(\lambda\nabla T)-\nabla(\rho_v V_v+\rho_v V_g)L-\nabla(\sum_{i=a,l,v}(T-T_r)\rho_i c_{pi}V_i) \quad (9)$$

2.2 Thermodynamic Relationship

The existence of a local equilibrium at any point within the porous is assumed. Kelvin's law is applied to the equation below.

$$h=exp\left(\frac{P_w-P_g}{\rho_l R_v T}\right) \quad (10)$$

The vapour partial pressure can be defined as a function of local temperature and relative humidity using equation below.

$$\rho_v=\rho_o h \quad (11)$$

where the saturation vapour pressure, ρ_o is estimated using equation in Mayhew[12] with saturated vapour density as a function of temperature. The degree of saturation, S is an experimentally determined function of capillary pressure and temperature.

$$S_l=S_l(p_c,T) \quad (12)$$

Saturation if expressed as combination of temperature effect[13] as in equation below.

$$S_l=\frac{\theta-\theta_r}{\theta_s-\theta_r}=\left(\frac{1}{1+(\alpha\varphi(T))^n}\right)^m \quad (13)$$

where the parameters α , n and m are dependent of porous material properties and influence the shape of the water retention curve. The permeability of water and gas are based on Muelem's model and given by the formulation below as in[14].

$$k_l(S_l)=\begin{cases}\sqrt{S_l}(1-(1-S_l^{\frac{1}{m}})^m)^2 & S_l > S_{irr}\\ 0 & S_l < S_{irr}\end{cases}$$

$$k_g(S_l)=\begin{cases}\sqrt{1-S_l}(1-S_l^{\frac{1}{m}})^m)^{2m} & S_l < S_{cri(g)}\\ 0 & S_l > S_{cri(g)}\end{cases} \quad (14)$$

2.3 Material Data

As mentioned in section 1, thin ceramic membrane that consist of two layering systems is presented as shown in Figure 2. In this study, porous slab (0.003 × 0.004 m) which had 12 elements and 51 nodes are assumed to be a porous medium that is homogeneous, isotropic and composed of solid phase, water and vapor phase, gas phase and dry air phase. Nodes 1 to 7 are assumed to be remained under atmospheric condition, while the rest of the wall surfaces are assumed to be insulated and impermeable. Hygroscopic layer for the simulation are located at elements 1, 5 and 9 while the rest of the elements are non hygroscopic layer. The ambient temperature is 27°C for slow convective drying with reference temperature at 25°C. Heat and mass coefficient are 1.5 W/m^{2}K and 0.00175 ms^{-1}. Material properties of these two different porous slab exposed to convective drying are listed in table 1.Material properties for hygroscopic and non hygroscopic layer are similar to alumina and clay ceramic profiles respectively.

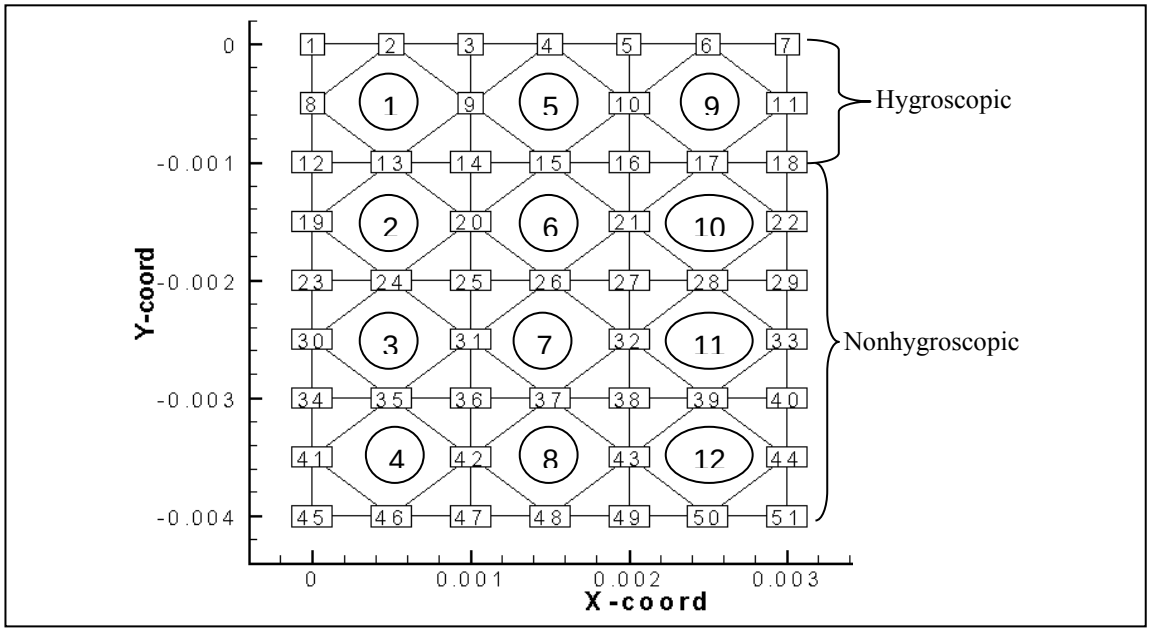

Figure 2 Mesh of the slab body

Table 1 Physical properties of material body for hygroscopic and non hygroscopic layer

Layer	Symbol	Value	Unit	Reference
Hygroscopic	ρ_s	3970	kg/m^3	Witharana *et al.* (2012)[15]
	$Ø$	0.1	-	Assumed by modeling and experimental data
	K	5.13 x 10^{-17}	m^2	Schmitz *et al.* (2012)[16]
	C_p	775	J/kg·K	Callister and Rethwisch (2011)[17]
	λ	39	W/m·K	Callister and Rethwisch (2011)[17]
Non hygroscopic	ρ_s	2000	kg/m^3	Harun and Gethin (2008)[7]
	$Ø$	0.4	-	Hall and Hoff (2012)[18]
	K	2.9 x 10^{-15}	m^2	Hall and Hoff (2012)[18]
	C_p	925	J/kg·K	Harun and Gethin (2008)[7]
	λ	1.8	W/m·K	Harun and Gethin (2008)[7]

2.4 Boundry Condition

In this work, two layer system based on hygroscopic and nonhygroscopic of membrane layering system were simulated as shown in Figure 2. The drying was imposed to the top surface of dense layer membrane that assigned as a hygroscopic materials and the rest of surfaces were assumed insulated. Thus, the boundary condition of convective drying is applied to element 1, 5 and 9 consists of node 1 until 7. The general boundary condition is applied for convective mass and heat transfer are given in the equations below.

$$J_m = h_m(P_\infty^v - P_a^v) \quad (15)$$

$$J_T = h_T(T_f - T_\infty) \quad (16)$$

2.5 Solution of Governing Equations and Numerical Method

The coupled heat and mass transfer equations described above, in 2-dimensions can be written into a matrix form as follows;

$$[C(\Phi)\frac{\partial}{\partial t}\{\Phi\} = \nabla([K_{cx}(\nabla\Phi)]i_x + [K_{cy}(\nabla\Phi)]i_y)\{\Phi\} + R(\nabla Z) \quad (17)$$

where$\{\Phi\} = \{P_w, T, P_g\}$ is the column of unknowns;[C],[K_{cx}]and [K_{cy}] are 3x3 matrices. Each element of the matrix is a coefficient for the unknown$\{\Phi\}$; i_x and i_y are the unit direction vectors. In order to discretize this simplified second order non-linear coupled partial differential equation, finite element method is used. Afterwards, Galerkin method is used to minimize the residual error before the application of Greens theorem, to the dispersive term involving second order derivatives; this simplified combined equation set can be expressed in the following form.

$$\underline{K}(\Phi)\underline{\Phi} + \underline{C}(\Phi)\dot{\Phi} + \underline{J}(\Phi) = \{0\} \quad (18)$$

where,

$$\underline{K} = \begin{bmatrix} \underline{K}_{11} & \underline{K}_{12} & \underline{K}_{13} & \underline{K}_{14} \\ \underline{K}_{21} & \underline{K}_{22} & \underline{K}_{23} & \underline{K}_{24} \\ \underline{K}_{31} & \underline{K}_{32} & \underline{K}_{33} & \underline{0} \end{bmatrix}$$

$$\underline{C} = \begin{bmatrix} \underline{C}_{11} & \underline{C}_{12} & \underline{C}_{13} \\ \underline{C}_{21} & \underline{C}_{22} & \underline{C}_{23} \\ \underline{C}_{31} & \underline{C}_{32} & \underline{C}_{33} \end{bmatrix}$$

$$\underline{J} = \begin{Bmatrix} \underline{J}_1 \\ \underline{J}_2 \\ \underline{J}_3 \end{Bmatrix} \qquad \underline{\Phi} = \begin{Bmatrix} \underline{P}_{ws} \\ \underline{T}_s \\ \underline{P}_{gs} \end{Bmatrix}$$

$$\dot{\underline{\Phi}} = \begin{Bmatrix} \frac{\partial \underline{P}_{ws}}{\partial t} \\ \frac{\partial \underline{T}_s}{\partial t} \\ \frac{\partial \underline{P}_{gs}}{\partial t} \end{Bmatrix}$$

In which typical elements of the matrix are

$$\underline{K}_{ij} = \sum_{s=1}^{n} \int_{\Omega^e} K_{ij} \nabla N_r \nabla N_s d\Omega^e$$

(i, j=1, 2,…., 5)

$$\underline{C}_{ij} = \sum_{s=1}^{n} \int_{\Omega^e} C_{ij} N_r N_s d\Omega^e$$

$$\underline{J}_i = \int_{\Omega^e} K_{i4} \nabla N_r \nabla z d\Omega^e - \int_{\Gamma^e} N_r \underline{J}_i d\Gamma^e$$

($\overline{n}$ - outward normal vector to the boundary, Γ of the domain Ω)

The transient matrix and nonlinear second order differential equations above are then solved by using a fully implicit backward time stepping scheme along with a Picard iterative method which is taken into account for non-linearity.

3.0 RESULTS AND DISCUSSION

Initially, the comparison of the proposed model which include hygroscopic equation and saturation results and compared with simulation results gained from Harun and Gethin[7] (nonhygroscopic), Przesmycki and Sturmillo[19] and Stanish *et al.*[20](hygroscopic) were conducted. Figure 3 shows the variation of average saturation generated by proposed model, simulation results gained from Harun and Gethin model[7], Przesmycki and Sturmillo[19] and Stanish *et al.*[20].

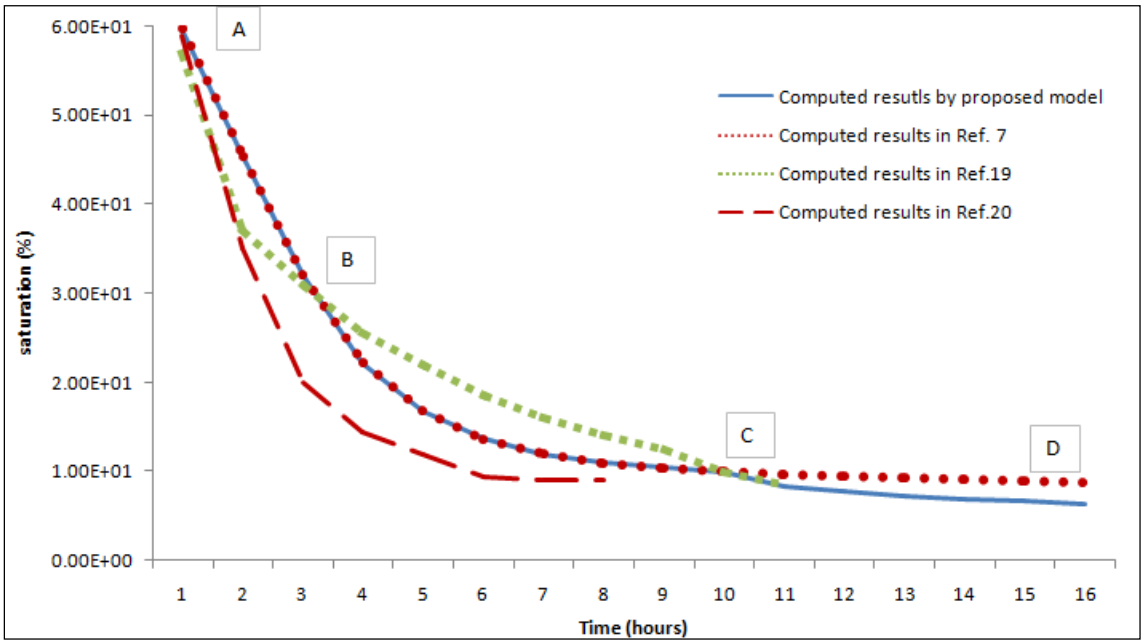

Figure 3 Saturation curve during drying

Obviously, Harun and Gethin[7] model and proposed model showed good agreement in the variations of saturation for drying period up to the nonhygroscopic zone in shell mould multilayer system. Presemycki and Sturmillo[19] that studied the drying of brick is in a close agreement for saturation evolution when drying period entered the hygroscopic zone. As for Stanish *et al.*[20], both proposed model and Stanish *et al.*[20] have similar saturation pattern but drying rates used by Stanish *et al.*[20] was faster compared to current model. Genarally, the saturation curve consists of three periods which CRP is indicated by a linear line from point A to B, FRP1 as gradual curve from point B to C and FRP2 by declining slope from point C to D (refer Figure 3). Explanation of all these periods of drying were discussed in detail in most drying phenomena of porous hygroscopic and nonhygroscopic materials.[3,4,5,7,8,10]

Figure 4 shows the variation of pore water pressure evolves with time and depth. Pore pressure water at the initial stages of drying shows a constant condition as free water is dominant during constant rate period[3,7,9] indicating free water continues been supply to the exposed surface by capillary action. The liquid migrates from regions with higher moisture concentration towards regions with lower moisture concentration as been expressed by Darcy's law[3]. This CRP can last as long as surface is supplied with liquid based on external factors and body properties.[3] When solid porous body is wet by liquid, it has a capillary adhesion that can holds particles together and it will weaken as liquid disappears during the drying.[9] Eventually, body may rupture during CRP when there is a drastic changes of pressure gradient in capillarity flow that will create nonhomogenous shrinkage.[9] When water saturation reaches the critical value that show the early stage of falling rate period, the pore water pressure shows an increasing trend due to increase of capillary action. This slightly higher value of pore pressure water within hygroscopic layer is due to greater capillary action of water that strongly attached to solid body and creates greater capillary suction. As the drying proceed towards irreducible stage, the pore water pressure is represent by bound water mechanism that dominated by vapour diffusion. The bound water removal stage for hygroscopic layer show an abrupt increased of pore water pressure especially at top surface indicate a greater capillary of bound water transfer near dryness.

The temperature variation over time and depth is shown in Figure 5. At the beginning stage of drying, temperature increased towards the ambient temperature as moisture removal is controlled by the external forces.[3] Heat energy supply from the surface towards the inner parts of the body will determine the drying rates.[3] For multilayer of hygroscopic and non hygroscopic, temperature profiles does not show any obvious trend[4] as there are slightly different in temperature changes within two layer. This small changes is impossible to be plot in the big scale of temperature. Therefore the curves are in constant trend. The temperatures profiles rise to higher value than the environment temperature when drying reaches falling rate period where gas diffusion takes places. Temperature inside the body reaches to it higher values as this generate greater diffusion process. With the increased of drying time, the temperature settling down towards the ambient temperature as no more energy is gained from the external environment. Drying state in current conditions is within internal forces such as bound water movement or sorption diffusion.[10] Temperature profiles during drying is particularly important to study especially when dealing with very thin layer of brittle ceramic membrane. This is due to the fact that the lower stresses induced due to small temperature gradient[9] could generate a massive expansion in ceramic membrane structure. Thereby, controlling the temperature is essential in order to avoid excessive stress, which would warp or crack the solid.

Gas pressure evolution against time and depth is showed in Figure 6. As shown in Figure 6, pressure gas remains at constant with atmosphere as results of free water capillary removal. Free water fills up the pores and drying rates is controlled by external heat and mass transfer.[3] As drying proceeds to the falling rate period, gas pressure starts to increase as pores liquid is replaced by gas. Diffusion of gases is important in this stage to enable

continues of mass transport towards the surface. Hence, this stage of drying is strongly affected by water vapour movement occurs by diffusion in respond to vapour pressure gradient. Top hygroscopic layer shows an increased trend of gas pressure due to smaller pores, higher density and small permeability value that restraint the gas movement to penetrate inside its body.[7] When it reaches non hygroscopic layer which material properties are opposed, the gas pressure seems to stay in constant condition as gases are trapped inside the body. Further drying causes the gas pressure to stabilize towards the ambient atmospheres pressure as less moisture to be dried. As drying reaches between the irreducible and equilibrium stage, gas phase or vapour pressure gradient is crucial towards bound water removal for hygroscopic material.[10] The gas pressure in hygroscopic layer reaches its highest value as gases penetrate through very fine capillaries[9] and remained stable when reaches non hygroscopic layer. Due to the fact that, during FRP, stress will induced due to macroscopic pressure gradient of escaping gasses.[9] Thereby, understanding the variation of gasses during drying and will help to reduce defects in membranes.

Figure 7 shows the saturation distributions as a function of depth and time. Saturation evolution shows moisture decreased very quickly at the early stage of drying. This movement of liquid is supplied by the capillary action as water continues to evaporate steadily. The surface of the material where heat is supplied to it is supposed to have higher liquid extraction rate.[4] In contrast to drying of single layer, saturation distribution for multilayer of hygroscopic materials does not showed any inclined curve as hygroscopic materials possesses small porous network. Saturation distribution pattern slowly reduced when drying reaches it critical stage which is normally 0.3 for porous materials.[10] Free water is getting lesser in this stage and diffusion of vapour is the main supplier of mass transfer within the body. When drying stage reaches the irreducible state which is 0.09 normally for non hygroscopic zone,[10] saturation is almost constant indicates there is no water can be removed as material been dried. This is shown in linear lines towards the later stage of drying. As for hygroscopic layer, bound water still exist within the body is continued been transport out with the help of vapour diffusion until it reaches the equilibrium content which a material can no more water can be remove under given situation.[10]

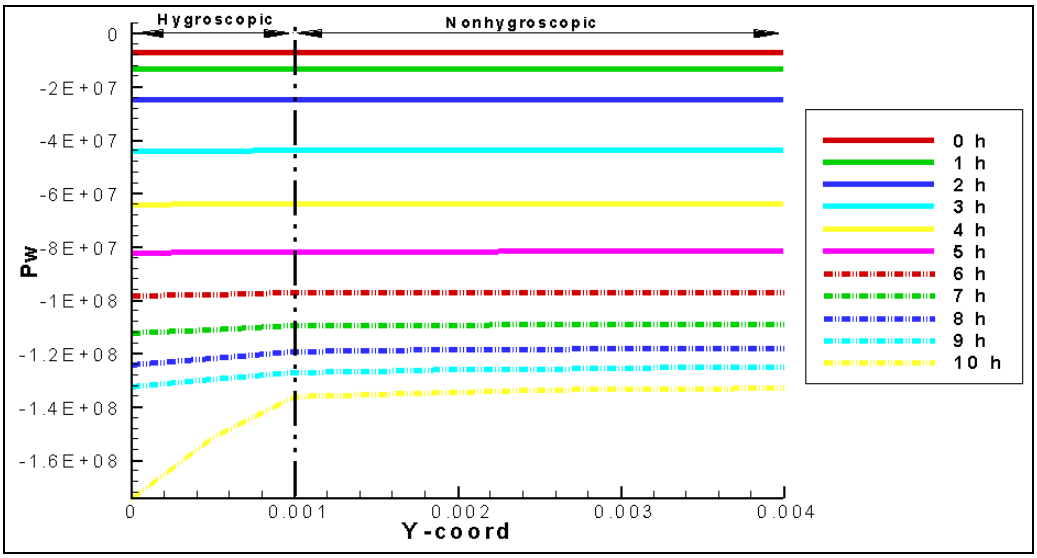

Figure 4 Pore water pressure distribution as a function of depth and time

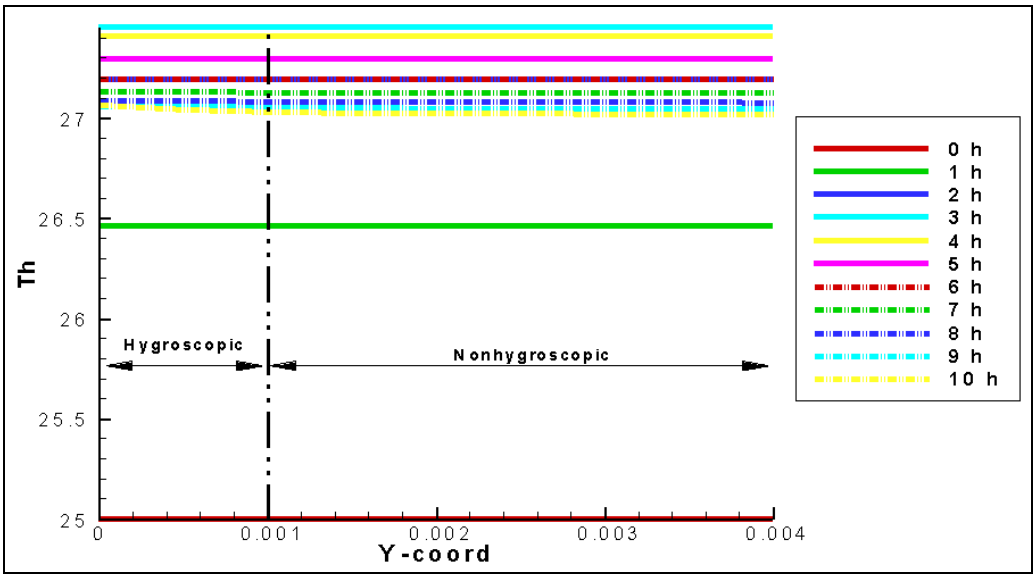

Figure 5 Temperature distribution as a function of depth and time

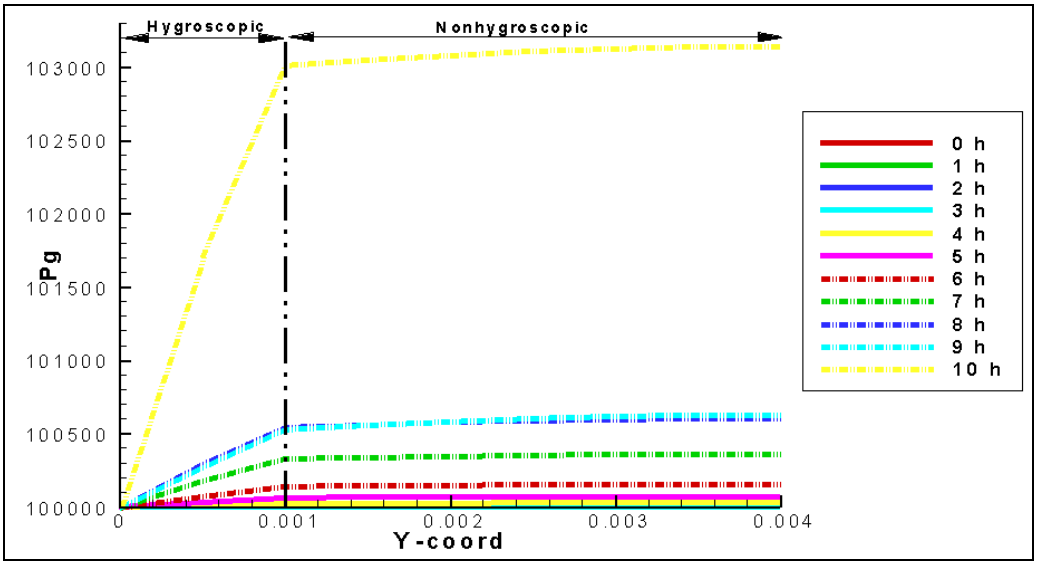

Figure 6 Gas pressure distribution as a function of depth and time

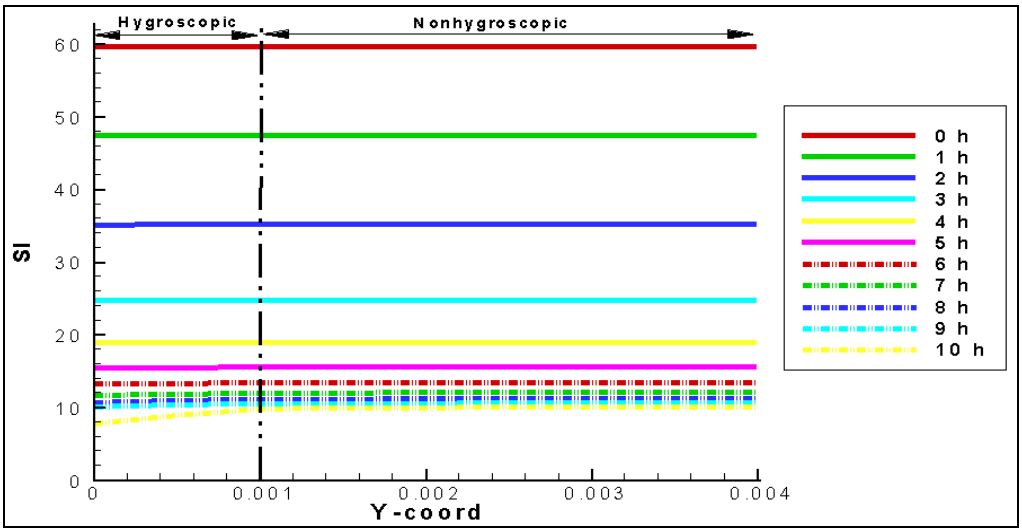

Figure 7 Saturation distribution as a function of depth and time

4.0 CONCLUSION

The effects of multilayer membranes structures varies greatly with different characteristic in drying compared to single material layer drying. The hygroscopic layer that inherited higher density, smaller permeability and smaller pores possesses higher pore water pressure and gas pressure. For hygroscopic materials, the bound water mechanism will take place with driving force in the gas phase or vapour pressure gradient. Stresses due to pressure gradient of liquid flow, macroscopic pressure gradient of escaping gasses and temperature gradient which causes defects such as cracking and warping on the separation layer of ceramic membranes can be avoided by having a better understanding of the drying process. Based on these simulated results, it can be concluded that better understanding of drying phenomena plays an important roles in predicting and determining the drying rate and process as well as drying transport diffusivity especially dealing with preparation of separation layer of ceramic membrane.

Acknowledgement

Authors thank to the financial support for LRGS Vot A022 grant and for the KPTM scholarship to Author 2.

Notations:
T = Temperature, K
P = pressure, Pa
V = velocity, ms^{-1}
ρ = density, kg/m^3
S = saturation
$\emptyset$ = porosity
C = heat capacity, J/(mol K)
θ = volumetric
K = intrinsic permeability, m^2
K = relative permeability
λ = thermal conductivity, W/mK
t = time , s
R = gas constant, J/(mol K)

Subscripts:
a, c, v, g, l, b = air, capillary, vapour, gas, liquid, bound water
s = saturated
irr = irreducible
cri = critical
r = residual

References

[1] K. Li. 2007. *Ceramic Membranes for Separation and Reaction*. Chichester: John Wiley & Sons Ltd. 59: 1–93.
[2] A. S. Mujumdar, Ed. 2006. *Handbook of Industrial Drying*. Boca Raton, USA: Taylor & Francis Group. 3.
[3] P. Perré, R. Remond, I. Turner. (M. A. Tsotsas, Evangelos, Ed.). 2007. *Modern Drying Technology*. Weinheim. Wiley VCH Verlag GmbH & Co. KGaA. 1–12.
[4] P. Rattanadecho, W. Pakdee, J. Stakulcharoen. 2007. *Drying Technology*. 26: 39–53.
[5] Z. Harun, N. M. Nawi, M. F. Batcha, D. T. Gethin. 2012. *Applied Mechanics and Materials*. 232: 548–552.
[6] N. F. Ismail, Z. Harun, N. A. Badarulzaman. 2012. *International Journal of Integrated Engineering*. 4–1: 16–21.
[7] Z. Harun, D. T. Gethin. 2008. *2nd Asia International Conference on Modelling and Simulation(AMS 2008)*. 794–799.
[8] Z. Harun, D. T. Gethin, R. W. Lewis. 2008. *The International Journal of Multiphysics*. 2: 1–19.
[9] T. A. Ring. 1996. *Fundamentals of Ceramic Powder Processing and Synthesis*. San Diego: Academic Press. 683–728.
[10] Z. Zhang, S. Yang, D. Liu. 1999. *Heat Transfer, Asian Research*. 28(5): 337–351.
[11] T. Defraeye, B. Blocken, D. Derome. 2012. *Chemical Engineering Science*. 32: 49–58.
[12] Y. R. Mayhew, G. F. C. Rogers. 1976. *Thermodynamic and Transport Properties of Fluids*. Oxford: Blackwell.
[13] M. V. Genuchten. 1980. *Soil Science Society of America Journal*. 8: 892–898.
[14] V. Baroghel-Bouny, M. Mainguy, T. Lassabatere, O. Coussy. 1999. *Cement and Concrete Research*. 29(8): 1225–1238.
[15] S. Witharana, C. Hodges, D. Xu, X. Lai, Y. Ding. 2012. *Journal of Nanoparticle Research*. 14(5): 851.
[16] A. V. Schmitz, Y. S. Mutlu, E. Glatt, S. Klein, B. Nestler. 2012. *Biomedizinische Technik. Biomedical Engineering*. 57 Suppl 1: 277–280.
[17] W. D. Callister, D. G. Rethwisch. 2011. *Materials Science and Engineering*. John Wiley & Sons, Inc. 8: 781–799.

[18] C. Hall, W. D. Hoff. 2012. *Water Transport in Brick, Stone and Concrete*. London: Spon Press. 2: 64–82.
[19] Z. Przesmycki, C. Strumillo. 1985. *Drying '85*. 126–134.
[20] M. A. Stanish, G. S. Schajer, F. Kayihan. 1986. *AIChE Journal*. 32(8): 1301–1311.